The Astrophysical Journal Letters, 777:L25 (6pp), 2013 November 10 doi:10.1088/2041-8205/777/2/L25

ALMA CONTINUUM OBSERVATIONS OF A 30 Myr OLD GASEOUS DEBRIS DISK AROUND HD 21997

A. Moór[1], A. Juhász[2], Á. Kóspál[3,10], P. Ábrahám[1], D. Apai[4], T. Csengeri[5], C. Grady[6,7], Th. Henning[8], A. M. Hughes[9], Cs. Kiss[1], I. Pascucci[4], M. Schmalzl[2], and K. Gabányi[1]

[1] Konkoly Observatory, Research Centre for Astronomy and Earth Sciences, Hungarian Academy of Sciences, P.O. Box 67, H-1525 Budapest, Hungary; moor@konkoly.hu
[2] Leiden Observatory, Leiden University, Niels Bohrweg 2, NL-2333-CA Leiden, The Netherlands
[3] Research and Scientific Support Department, European Space Agency (ESA-ESTEC, SRE-SA), P.O. Box 299, 2200-AG Noordwijk, The Netherlands
[4] Department of Astronomy and Department of Planetary Sciences, The University of Arizona, Tucson, AZ 85721, USA
[5] Max-Planck-Institut für Radioastronomie, Auf dem Hügel 69, D-53121 Bonn, Germany
[6] NASA Goddard Space Flight Center, Code 667, Greenbelt, MD 20771, USA
[7] Eureka Scientific, 2452 Delmer Street, Suite 100, Oakland, CA 94602, USA
[8] Max-Planck-Institut für Astronomie, Königstuhl 17, D-69117 Heidelberg, Germany
[9] Wesleyan University Department of Astronomy, Van Vleck Observatory, 96 Foss Hill Dr., Midletown, CT 06457, USA
Received 2013 July 24; accepted 2013 September 30; published 2013 October 23

ABSTRACT

Circumstellar disks around stars older than 10 Myr are expected to be gas-poor. There are, however, two examples of old (30–40 Myr) debris-like disks containing a detectable amount of cold CO gas. Here we present Atacama Large Millimeter/Submillimeter Array (ALMA) and *Herschel Space Observatory* observations of one of these disks, around HD 21997, and study the distribution and origin of the dust and its connection to the gas. Our ALMA continuum images at 886 μm clearly resolve a broad ring of emission within a diameter of $\sim$4.″5, adding HD 21997 to the dozen debris disks resolved at (sub)millimeter wavelengths. Modeling the morphology of the ALMA image with a radiative transfer code suggests inner and outer radii of $\sim$55 and $\sim$150 AU, and a dust mass of 0.09 $M_{\oplus}$. Our data and modeling hints at an extended cold outskirt of the ring. Comparison with the morphology of the CO gas in the disk reveals an inner dust-free hole where gas nevertheless can be detected. Based on dust grain lifetimes, we propose that the dust content of this gaseous disk is of secondary origin and is produced by planetesimals. Since the gas component is probably primordial, HD 21997 is one of the first known examples of a hybrid circumstellar disk, a thus-far little studied late phase of circumstellar disk evolution.

Key words: circumstellar matter – infrared: stars – stars: individual (HD 21997)

Online-only material: color figures

1. INTRODUCTION

Circumstellar disks around stars older than 10 Myr are expected to be gas-poor. By that time, the massive gaseous *primordial* disks, natural by-products of star formation and potential birthplaces of planetary systems, are largely depleted. They evolve into tenuous *debris* disks, composed of second-generation dust grains produced from collisional erosion and/or evaporation of previously formed planetesimals (Wyatt 2008). Debris disks are thought to have an extremely low gas-to-dust ratio compared to primordial disks. Gas in these systems—if it exists at all—may also be second-generation, produced from icy planetesimals/grains (e.g., Vidal-Madjar et al. 1994; Grigorieva et al. 2007; Czechowski & Mann 2007). However, we know of two circumstellar disks—around the $\sim$30 Myr old, A3-type HD 21997 (Moór et al. 2011a) and the $\sim$40 Myr old, A1-type 49 Ceti (Zuckerman et al. 1995; Hughes et al. 2008)—that harbor detectable amounts of CO gas revealed by millimeter observations, while at the same time infrared observations show debris-like dust content. The origin of the gas in these systems is hotly debated. Zuckerman & Song (2012) proposed that the observed CO may be released from colliding comets thus it would have a secondary origin. By modeling the gas observations of 49 Ceti, Roberge et al. (2013) also suggested that the gas may be secondary material. Although the ages of these systems significantly exceed both model predictions for disk clearing and the ages of the oldest transitional disks, the gas may still be residual primordial material that survived longer in the outer disks than is usually assumed (e.g., Krivov et al. 2009).

Gas around HD 21997 has recently been discovered (Moór et al. 2011a). At a distance of 72 pc, HD 21997 belongs to the 30 Myr old Columba association (Moór et al. 2006; Torres et al. 2008). By modeling the spectral energy distribution (SED) and the single-dish CO measurements available at the time, we could not determine the spatial distribution of gas and dust unambiguously due to the unknown inclination and the degeneracy between grain size and location. To study the temperature and density structure of the circumstellar matter, the physical interaction between gas and dust, and the origin of the gas, spatially resolved observations are indispensable. In this Letter, we present the first spatially resolved continuum image of HD 21997 with the Atacama Large Millimeter/Submillimeter Array (ALMA) at 886 μm. These data were supplemented by far-infrared/submillimeter measurements obtained with the *Herschel Space Observatory* (Pilbratt et al. 2010). In order to study the gas properties in the disk, we also observed CO lines with ALMA, presented in Kóspál et al. (2013).

2. OBSERVATIONS AND DATA REDUCTION

2.1. ALMA Observations

We observed the continuum emission from HD 21997 as part of our ALMA Early Science Cycle 0 program (PI: Á. Kóspál, project ID: 2011.0.00780.S). Observations were executed on

[10] ESA fellow.

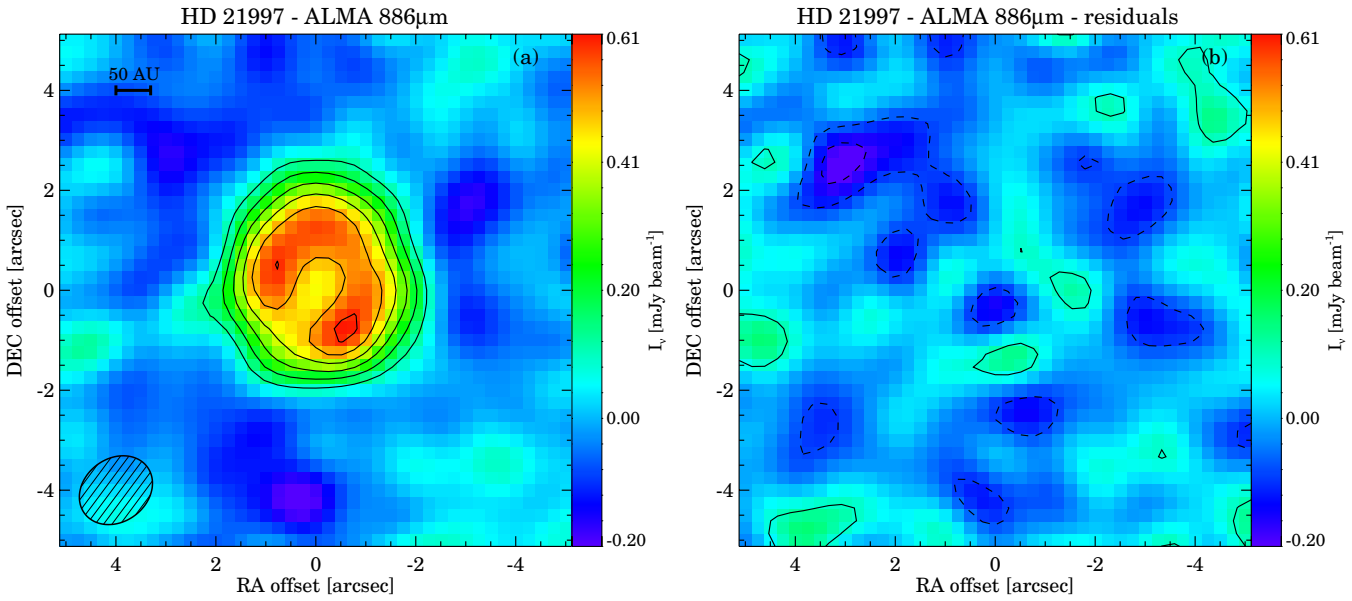

Figure 1. (a) 886 μm continuum map, contours indicate [3, 5, 7, 9, 11, 13] $\times\,\sigma$ level intensities. The ellipse in the lower left corner indicates the beam. The 0, 0 coordinates correspond to the stellar position. (b) Residuals after subtracting our extended model, with contours $[-4, -2, 2]\times\sigma$.
(A color version of this figure is available in the online journal.)

2011 November 4 in a compact configuration using 15 antennas, with low spectral resolution (time division mode, TDM) offering baselines from 18.3 m to 134.2 m. Four spectral windows with a bandwidth of 2 GHz each were defined around 345 GHz. The total on-source exposure time was ≈2 hr. J0403–360 served as bandpass calibrator, while Callisto was used to constrain the absolute amplitude scale. Our project also included high spectral resolution line observations of HD 21997 around 330–345 GHz in frequency division mode (FDM), described in Kóspál et al. (2013). In order to increase the signal-to-noise ratio, we extracted the continuum emission from the FDM data using line-free channels, and concatenated these with our TDM measurements using appropriate weighting. The effective wavelength of the combined data set is 886 μm. The TDM and FDM maps are consistent in terms of flux level. We performed imaging with the multi-frequency synthesis algorithm with the Common Astronomy Software Applications (CASA) v3.3 task CLEAN. The image (Figure 1(a)) has a typical rms noise of 4.5×10^{-2} mJy beam^{-1}, a beam size of $1\farcs56\times1\farcs26$, and a beam position angle (P.A.) of $-53\fdg4$.

2.2. Herschel Observations

We obtained far-infrared and submillimeter maps of HD 21997 (OT1_pabraham_2, PI: P. Ábrahám) using the Photodetector Array Camera and Spectrometer (PACS; Poglitsch et al. 2010) and the Spectral and Photometric Imaging Receiver (SPIRE; Griffin et al. 2010) onboard *Herschel*. PACS observations were carried out on 2012 January 13 in the mini scan-map mode, using medium scan speed ($20''$ s^{-1}) and scan angles of 70° and 110° both in the blue (70 μm) and green (100 μm) bands, repeated four times in each scan direction. This setup provided 16 maps at 160 μm as well. PACS data were reduced with the Herschel Interactive Processing Environment (HIPE; Ott 2010) v9.2, applying the standard pipeline steps. We removed $1/f$ noise by applying highpass filtering while the immediate vicinity of our target was masked out to avoid flux loss. We used second-level deglitching to remove glitches. We produced 8, 8, and 16 individual maps using the PHOTPROJECT task with pixel sizes of $1\farcs1$, $1\farcs4$, and $2\farcs1$ at 70, 100, and 160 μm (the FWHM beam sizes at these wavelengths are $\sim5\farcs6$, $\sim6\farcs8$, and $\sim11\farcs3$, respectively). Finally, we created mosaics in each band, by averaging the individual scan maps.

SPIRE observations were performed on 2012 January 28 in the Small Scan Map mode resulting in simultaneous 250, 350, and 500 μm maps. We reduced the data with HIPE v9.2 using the standard pipeline script. The pixel sizes of the maps are $6''$, $10''$, and $14''$, while the beam sizes are $\sim18\farcs2$, $\sim24\farcs9$, and $\sim36\farcs3$ at 250, 350, and 500 μm, respectively.

2.3. Spitzer/IRS Observations

HD 21997 was observed with the InfraRed Spectrograph (IRS; Houck et al. 2004) onboard the *Spitzer Space Telescope* on 2004 January 5. Small 2 × 3 maps were taken with the low-resolution IRS modules, covering the 5.2–38 μm range. We downloaded the data processed with the pipeline version S18.18.0 from the *Spitzer* archive and further processed them with the Spitzer IRS Custom Extraction Software (SPICE v2.5.0). We used the two central map positions and subtracted them from each other. Then, we extracted the positive signal from a wavelength-dependent, tapered aperture, and averaged them. The final spectrum is plotted in Figure 2(a).

3. RESULTS AND ANALYSIS

3.1. ALMA Image

At 886 μm the disk emission is clearly detected and resolved into a ring-like structure encircling the stellar position (Figure 1(a)). The peak signal-to-noise ratio along the ring is 13.4. In order to analyze the ring morphology, in Figure 1(a) we made cuts from the stellar position toward different position angles between 0° and 360° in 10° increments and determined the location of maximum intensity along the cuts. These points could be fitted with an ellipse with major and minor axes of $2\farcs06\times1\farcs73$ and a P.A. of $21\fdg5\pm3\fdg5$, measured from north to east. Assuming an intrinsically circular ring, we derived an

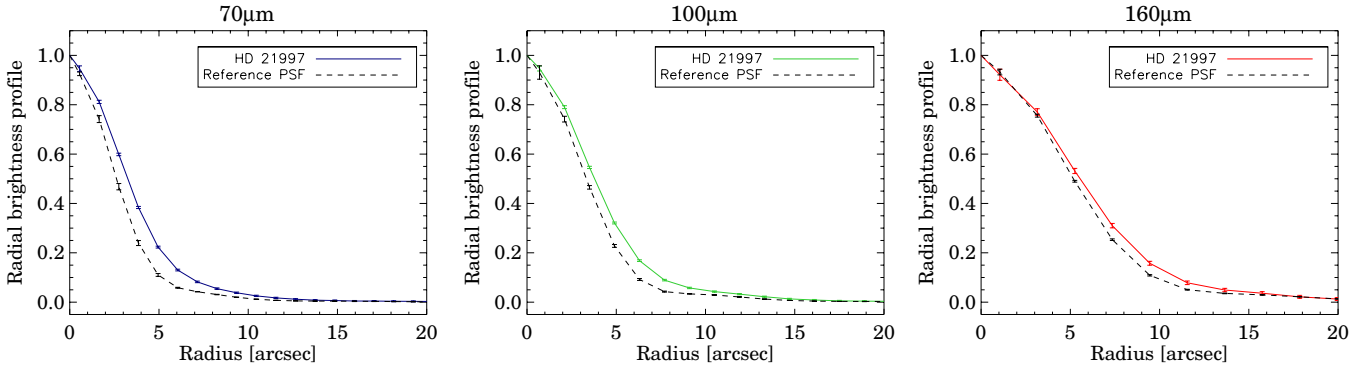

Figure 2. Radial brightness profiles for HD 21997 and reference PSF profiles (see Section 3.2).
(A color version of this figure is available in the online journal.)

inclination of $32.^{\circ}9 \pm 2.^{\circ}6$ (measured from pole-on). The analysis of CO line data provided similar estimates for these parameters (P.A. $= 22.^{\circ}6 \pm 0.^{\circ}5$, $i = 32.^{\circ}6 \pm 3.^{\circ}1$; Kóspál et al. 2013). The emission above 3σ level can be detected within a diameter of $4.''5$.

The intensity profile along the perimeter has several localized peaks. To decide whether these peaks are real, possibly implying a non-axisymmetric dust distribution, we computed the standard deviation of the intensity profile along the fitted ellipse and compared its value, 4.1×10^{-2} mJy beam^{-1}, to the 1σ noise of the continuum map of 4.5×10^{-2} mJy beam^{-1}. This suggests that none of the peaks are significant. We also defined a number of ellipses of the same size and orientation as the fitted one in different emission-free parts of the map. We compared the intensity profiles of these ellipses with that measured along the ring, and found that brightness fluctuations responsible for the observed local peaks exist in the background, too. In conclusion, there is no observational evidence for any azimuthal asymmetry in the ring.

We integrated the emission within a circular aperture with a radius of $2.''8$ centered on the stellar position, and obtained 2.69 ± 0.30 mJy for the total continuum flux of the dust disk. The uncertainty includes 10% calibration uncertainty.

3.2. Herschel PACS and SPIRE Maps

Figure 2 shows the azimuthally averaged radial brightness profiles of the source and reference point-spread functions (PSFs) at all PACS wavelengths. The PSFs were constructed using PACS observations of two calibrator stars (α Boo and α Tau), performed and processed in the same way as HD 21997 and rotated to match the roll angle of the telescope at the time of observing HD 21997. As Figure 2 demonstrates, the disk is marginally resolved at all wavelengths. We fitted elliptical Gaussians to the source and PSFs, and used quadratic deconvolution to derive the target's FWHM sizes, yielding $4.''7 \pm 0.''1 \times 4.''3 \pm 0.''2$, $4.''7 \pm 0.''2 \times 4.''1 \pm 0.''2$, and $5.''5 \pm 1.''1 \times 4.''5 \pm 0.''9$ at 70, 100, and 160 μm, respectively. The derived position angles at 70 and 100 μm are $20.^{\circ}9 \pm 8.^{\circ}1$ and $25.^{\circ}9 \pm 9.^{\circ}3$. Assuming an azimuthally symmetric structure, the inclination of the disk is $25.^{\circ}1 \pm 5.^{\circ}7$, $29.^{\circ}8 \pm 5.^{\circ}5$.

We performed aperture photometry using an aperture radius of $20''$ and sky annulus between $40''$ and $50''$. The aperture was placed at the measured photocenter of the source. We averaged flux densities measured in individual scan maps (8, 8, and 16 values at 70, 100, and 160 μm) and computed their rms. Fluxes were aperture corrected and the final uncertainties of the photometry were computed by adding quadratically the measurement errors and absolute calibration uncertainty of 7% (Balog et al. 2013).

We performed aperture photometry for HD 21997 in the SPIRE maps with a circular aperture of $22''$, $30''$, and $42''$ at 250, 350, and 500 μm. The background levels were estimated in annuli between $60''$ and $90''$. The final uncertainties are the quadratic sum of the measurement errors and the overall calibration uncertainty of 5.5% for SPIRE (Bendo et al. 2013).

The obtained ALMA and *Herschel* flux densities and their uncertainties are listed in Table 1.

3.3. Modeling of Dust Distribution

As preparation for modeling the morphology of the dust disk, we compiled the SED of the source using data from the literature and our new *Herschel* and ALMA observations. For the fitting process, the IRS spectra were sampled in 11 adjacent bins using the same method as in Moór et al. (2011b). Table 1 summarizes these photometric data. A stellar photosphere model with a luminosity of 11.3 $L_{\odot}$ was taken from Moór et al. (2011a). The SED in Figure 3(a) shows that at most wavelengths the flux densities measured by different instruments are consistent; however, our ALMA flux diverges from the trend delineated by non-interferometric submillimeter observations. The 886 μm ALMA flux is only ~30% of the flux measured with SCUBA at 850 μm (with an FWHM of $14.''5$) and of the 886 μm flux extrapolated from the SPIRE observations. This is not a calibration issue, because our ALMA line observations agree well with our previous APEX measurements (Kóspál et al. 2013), and the continuum maps created from FDM and TDM data, obtained on different epochs, also provide fluxes consistent within 8%. Since there are no additional sources in the vicinity of HD 21997 in the PACS and ALMA images, we suspect that this flux loss occurred because some extended emission was filtered out by the ALMA interferometer.

3.3.1. Simple Model

We first deprojected the ALMA visibilities using the disk inclination and position angle derived in Section 3.1 and then radially averaged in 7 kλ wide bins. Figure 3(b) displays the real and imaginary components of the binned fluxes. The DEBris disk RAdiative transfer code (DEBRA; Olofsson et al. 2012), developed for optically thin radiation, was used to model the visibilities. The code was extended with a ray-tracer to calculate images for ALMA simulations. HD 21997 has a featureless mid-infrared spectrum, providing no information

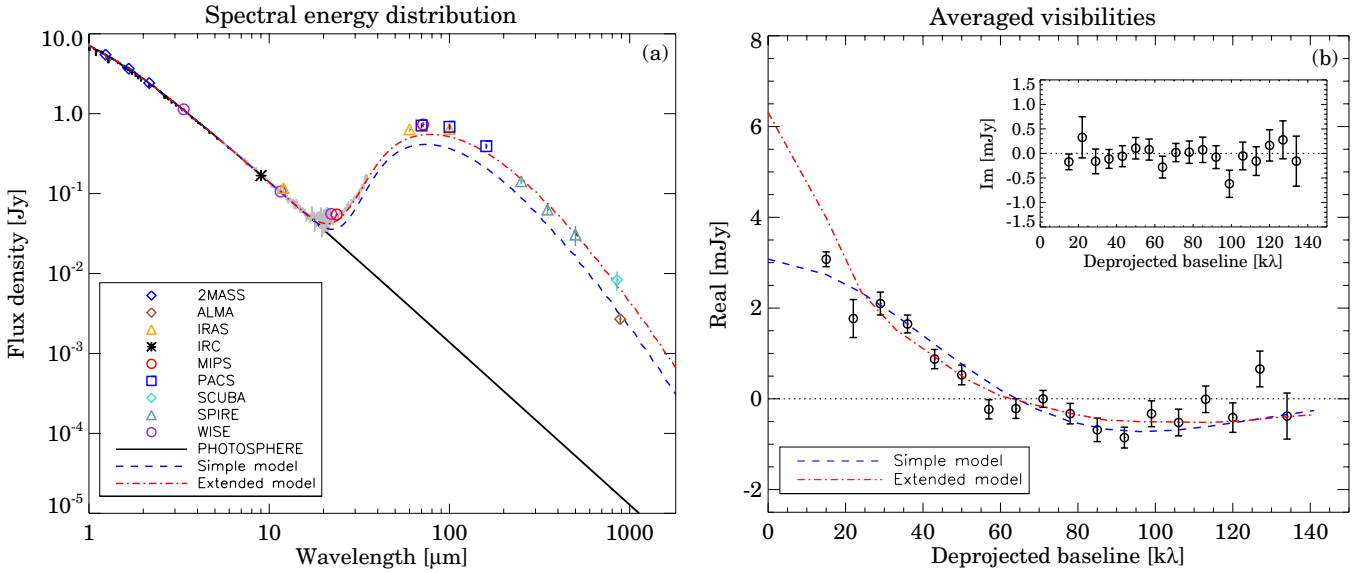

Figure 3. (a) Color corrected SED of the source. (b) Real and imaginary (inset) components of the deprojected ALMA continuum visibilities.
(A color version of this figure is available in the online journal.)

Table 1
Measured and Predicted Fluxes

Wavelength (μm)	Measured Flux Density (mJy)	Instrument	Predicted Flux Density (mJy)	Reference
3.35	1129.0 ± 51.4	*WISE*	1116.3	Wright et al. (2010)
8.86	179.2 ± 27.0	IRS	176.7	This work
9.00	200.4 ± 22.2	IRC	171.3	Ishihara et al. (2010)
11.02	116.0 ± 12.6	IRS	115.0	This work
11.56	106.6 ± 5.2	*WISE*	104.7	Wright et al. (2010)
12.00	173.0 ± 19.0	*IRAS*	97.3	Moshir (1989)
13.02	83.8 ± 9.3	IRS	82.8	This work
14.90	65.2 ± 7.6	IRS	63.4	This work
16.99	52.4 ± 5.8	IRS	48.9	This work
19.12	50.2 ± 7.3	IRS	38.8	This work
21.08	47.0 ± 8.6	IRS	31.9	This work
22.09	57.2 ± 3.7	*WISE*	29.1	Wright et al. (2010)
23.67	55.1 ± 2.2	MIPS	25.3	Moór et al. (2011a)
24.48	55.1 ± 4.9	IRS	23.6	This work
27.45	70.1 ± 8.2	IRS	18.8	This work
30.50	92.3 ± 10.3	IRS	15.2	This work
33.44	134.3 ± 23.2	IRS	12.6	This work
60.00	595.0 ± 35.7	*IRAS*	3.9	Moshir (1989)
70.00[a]	697.6 ± 49.2	PACS	2.8	This work
71.42	663.7 ± 46.9	MIPS	2.7	Moór et al. (2011a)
100.00	636.0 ± 108.1	*IRAS*	1.4	Moshir (1989)
100.00[a]	665.4 ± 47.5	PACS	1.4	This work
160.00[a]	410.8 ± 30.0	PACS	0.5	This work
250.00	151.4 ± 11.0	SPIRE	0.21	This work
350.00	66.7 ± 9.5	SPIRE	0.11	This work
500.00	33.1 ± 9.4	SPIRE	0.05	This work
850.00	8.3 ± 2.3	SCUBA	0.02	Williams & Andrews (2006)
886.00[a]	2.69 ± 0.30	ALMA	0.02	This work

Note. [a] The emission is spatially resolved at these wavelengths.

about dust composition. Dust particles were assumed to be a mixture of amorphous silicates with olivine stoichiometry and amorphous carbon. The optical constants of silicate and carbon were taken from Dorschner et al. (1995) and Jäger et al. (1998), respectively, while mass absorption and scattering coefficients were calculated using Mie-theory. The dust size distribution was assumed to be a power law with an exponent of −3.5, characteristic of collisionally dominated systems. The maximum grain size ($s_{\rm max}$) was fixed at 3000 μm, the minimum grain size ($s_{\rm min}$) was varied by setting 4, 6, 8, and 16 μm. The model disk had a power-law surface density distribution between an inner ($R_{\rm in}$) and outer radius ($R_{\rm out}$). We calculated a grid of models varying $R_{\rm in}$, $R_{\rm out}$, and the surface density exponent (p). The best-fit solution and the corresponding errors were derived

using a marginal likelihood estimator, calculated from the χ^2 of the fit of individual models. We determined best-fit models for each dust size distribution and compared the model SEDs with the observations. This comparison excluded $s_{\rm min} = 4$ μm for its incompatibility with mid-infrared data. Our best-fit solution, plotted in Figures 3(a) and (b), has $R_{\rm in} = 62 \pm 13$ AU, $R_{\rm out} = 150 \pm 47$ AU, $p = -2.4 \pm 4.5$, $s_{\rm min} = 6$ μm, and $M_{\rm dust} = 0.09 \pm 0.03\,M_{\oplus}$.

3.3.2. Extended Model

As Figure 3(a) shows, our best-fit model underestimates the observed fluxes at most wavelengths. Moreover, the simulated PACS images—calculated by convolving our model with the appropriately rotated PACS PSFs—are less extended than the measured ones. These discrepancies hint at a cold outer extension of the disk. To test this hypothesis, we fitted the SED, the PACS profiles, and the ALMA visibilities simultaneously. The ALMA flux was discarded from the SED fitting since it suffers from spatial filtering. We used DEBRA with the same modeling setup as above. We combined χ^2 values of the SED and ALMA visibilities with equal weight and performed a consistency check on the PACS images. The best-fit solution was reached with $R_{\rm in} = 55 \pm 16$ AU, $p = -1.6 \pm 0.8$, $M_{\rm dust} = 0.27 \pm 0.11\,M_{\oplus}$, and $s_{\rm min} = 6$ μm. $R_{\rm out}$ cannot be constrained by the ALMA visibilities, and models that reproduce the SCUBA flux and having $R_{\rm out} > 490$ AU are all consistent with the data within the uncertainties. Our best-fit SED and visibility models with $R_{\rm out} = 490$ AU are plotted in Figures 3(a) and (b). The fit reproduces both the long wavelength data points and visibilities and, moreover, between ~55 and 150 AU it is consistent within uncertainties with our previous model. Furthermore, consistently with the IRS spectrum, our model does not show silicate features at mid-infrared wavelengths. Thus, our modeling suggests the existence of a cold extended component, but its physical parameters are only weakly constrained by our data.

4. DISCUSSION

A special feature of the HD 21997 disk is its substantial molecular gas content. Using ALMA, Kóspál et al. (2013) resolved the disk in $J = 2$–1 and $J = 3$–2 transitions of ^{12}CO and ^{13}CO and in $J = 2$–1 transition of C^{18}O. They found that the observed CO brightness distribution could be reproduced by a simple disk model with inner and outer radii of <26 AU and 138 ± 20 AU. The inner radius of the dust disk, $R_{\rm in} = 55 \pm 16$ AU is larger than the quoted 1σ upper limit of the gas inner radius at a 1.8σ level, implying that there probably is a dust-poor inner region and gas and dust may only be co-located between ~55 AU and ~140 AU. The differences in the inner disk morphologies can also be visualized by comparing our Figure 1(a) with Figure 2 (left) in Kóspál et al. (2013). Our extended modeling also implies the existence of an outer dust halo.

The total CO mass was estimated to be 0.04–0.08 $M_{\oplus}$ based on optically thin C^{18}O observation (Kóspál et al. 2013). If the gas is of secondary origin, produced from icy planetesimals/grains, then the total gas mass is of the same order of magnitude as the CO mass. This would yield a gas-to-dust mass ratio of ~0.4 in the co-located region. However, in Kóspál et al. (2013) we found that this scenario could not explain satisfactorily the difference in gas/dust spatial distribution and would require an unreasonably high gas production rate, implying that the gas is more likely of residual primordial origin. In this case, H_2 is also expected in the disk, and assuming a canonical CO/H_2 ratio of 10^{-4}, the total gas mass would be 30–60 $M_{\oplus}$. This gives a gas-to-dust mass ratio of ~300 in the co-located region. One reason for this high value could be that most of the dust ended up in planetesimals that cannot be detected at submillimeter wavelengths.

Our extended model gives a fractional luminosity of 4.8×10^{-4} and a dust temperature range between 20 and 100 K. Thus, the fundamental properties of the HD 21997 disk are similar to those of other young debris disks. The primordial gas scenario, however, raises the question of whether the dust grains are really secondary, since gas could dampen impact velocities between dust particles, thereby increasing their lifetime in regions where both gas and dust are present. Gas in such a disk is orbiting at sub-Keplerian velocities due to a radial pressure gradient. Dust grains also orbit with sub-Keplerian velocity but their pace depends on size and composition. The velocity difference between gas and dust induces grain migration within the disk (Takeuchi & Artymowicz 2001; Krivov et al. 2009). Grains with angular velocities larger/smaller than that of the gas lose/gain angular momentum and drift inward/outward until they are in corotation with the gas. Based on their models, Krivov et al. (2009) found that even in gaseous debris disks with a gas-to-dust mass ratio of 100, the grains' lifetime will be very limited—typically less than 2×10^4 yr—because collisions occur between radially drifting grains with unequal sizes. Applying these findings for the case of HD 21997, we conclude that the grains must be replenished and are of secondary origin. The lack of spectral features from small particles in the IRS spectrum—unlike in Herbig Ae and transitional disks where grains are mainly primordial—and the dominance of large grains ($\gtrsim 6$ μm, Section 3.3) similarly to other debris disks also supports this conclusion.

Emission at (sub)millimeter wavelengths predominantly comes from large grains with a size >100 μm. In a gas-free debris disk, such large grains are little affected by radiative forces, thus, they trace the distribution of the parent planetesimals (Wyatt 2008). In the secondary gas scenario of HD 21997 the models of Takeuchi & Artymowicz (2001) predict only weak coupling between gas and grains of >100 μm, thus, grain migration is negligible. This implies a radially broad planetesimal belt in the HD 21997 system. For destructive collisions between planetesimals, collision velocity must exceed a critical value that requires a dynamically excited (stirred) environment. In the *self-stirring* model (Kenyon & Bromley 2008), the formation of >1000 km sized planetesimals can initiate a collisional cascade in those disk regions where they appeared. Since the formation of such oligarchs takes longer at larger radii, the site where active dust production occurs is expected to propagate outward. Based on formulae from Kenyon & Bromley (2008), even in a disk with a surface density 10 times higher than the minimum-mass solar nebula, the formation of large oligarchs can spread out only to ~90 AU within 30 Myr. The dust disk (and the planetesimal belt) of HD 21997 extends out to $\gg$90 AU, which cannot be explained via self-stirring. In this case, planetary stirring (Mustill & Wyatt 2009) may be a viable alternative stirring mechanism to explain the dynamical excitation in the outer regions. If a large amount of primordial gas is present (our favored scenario), the gas–dust coupling is stronger and it might induce radial migration of grains. Therefore, in the primordial gas scenario, it is possible that HD 21997 has a narrower planetesimal ring, and the extended morphology of the dust is explained by efficient

grain migration. However, the details of grain migration (e.g., the magnitude of migration) cannot be reliably constrained by the available data, therefore we cannot judge the viability of this scenario.

Our study indicates that the dust content of the disk is of secondary origin while Kóspál et al. (2013) claims that the gas component is more likely primordial. We know of several young circumstellar disks that dominantly contain primordial gas and dust, but in their innermost region may have debris dust as well (e.g., Grady et al. 2009; Roberge et al. 2005; Eisner et al. 2006). HD 21997 may be a more evolved *hybrid disk* where the dust component is mainly made of second generation material.

We thank our anonymous referee whose comments improved the manuscript. This Letter makes use of the following ALMA data: ADS/JAO.ALMA#2011.0.00780.S. ALMA is a partnership of ESO (representing its member states), NSF (USA) and NINS (Japan), together with NRC (Canada) and NSC and ASIAA (Taiwan), in cooperation with the Republic of Chile. The Joint ALMA Observatory is operated by ESO, AUI/NRAO, and NAOJ. This research was partly funded by the Hungarian OTKA grants K101393/K104607 and the PECS-98073 program of the European Space Agency (ESA). A.M. and C.K. acknowledge the support of the Bolyai Fellowship. K.G. acknowledges support from the Hungarian OTKA grant NN102014.

Facilities: ALMA, *Herschel*

REFERENCES

Balog, Z., Müller, T., Nielbock, M., et al. 2013, arXiv:1309.6099
Bendo, G. J., Griffin, M. J., Bock, J. J., et al. 2013, MNRAS, 433, 3062
Czechowski, A., & Mann, I. 2007, ApJ, 660, 1541
Dorschner, J., Begemann, B., Henning, T., Jaeger, C., & Mutschke, H. 1995, A&A, 300, 503
Eisner, J. A., Chiang, E. I., & Hillenbrand, L. A. 2006, ApJL, 637, L133
Grady, C. A., Schneider, G., Sitko, M. L., et al. 2009, ApJ, 699, 1822
Griffin, M. J., Abergel, A., Abreu, A., et al. 2010, A&A, 518, L3
Grigorieva, A., Thébault, P., Artymowicz, P., & Brandeker, A. 2007, A&A, 475, 755
Houck, J. R., Roellig, T. L., van Cleve, J., et al. 2004, ApJS, 154, 18
Hughes, A. M., Wilner, D. J., Kamp, I., & Hogerheijde, M. R. 2008, ApJ, 681, 626
Ishihara, D., Onaka, T., Kataza, H., et al. 2010, A&A, 514, A1
Jäger, C., Mutschke, H., & Henning, T. 1998, A&A, 332, 291
Kenyon, S. J., & Bromley, B. C. 2008, ApJS, 179, 451
Kóspál, Á., Moór, A., Juhász, P., et al. 2013, ApJ, 776, 77
Krivov, A. V., Herrmann, F., Brandeker, A., & Thébault, P. 2009, A&A, 507, 1503
Moór, A., Ábrahám, P., Derekas, A., et al. 2006, ApJ, 644, 525
Moór, A., Ábrahám, P., Juhász, A., et al. 2011a, ApJL, 740, L7
Moór, A., Pascucci, I., Kóspál, Á., et al. 2011b, ApJS, 193, 4
Moshir, M. 1989, Explanatory Supplement to the IRAS Faint Source Survey (Pasadena, CA: JPL)
Mustill, A. J., & Wyatt, M. C. 2009, MNRAS, 399, 1403
Olofsson, J., Juhász, A., Henning, T., et al. 2012, A&A, 542, A90
Ott, S. 2010, in ASP Conf. Ser. 434, Astronomical Data Analysis Software and Systems XIX, ed. Y. Mizumoto, K.-I. Morita, & M. Ohishi (San Francisco, CA: ASP), 139
Pilbratt, G. L., Riedinger, J. R., Passvogel, T., et al. 2010, A&A, 518, L1
Poglitsch, A., Waelkens, C., Geis, N., et al. 2010, A&A, 518, L2
Roberge, A., Kamp, I., Montesinos, B., et al. 2013, ApJ, 771, 69
Roberge, A., Weinberger, A. J., & Malumuth, E. M. 2005, ApJ, 622, 1171
Takeuchi, T., & Artymowicz, P. 2001, ApJ, 557, 990
Torres, C. A. O., Quast, G. R., Melo, C. H. F., & Sterzik, M. F. 2008, in Handbook of Star Forming Regions, Volume II: The Southern Sky, ed. B. Reipurth (ASP Monograph Publications, Vol. 5; San Francisco, CA: ASP), 757
Vidal-Madjar, A., Lagrange-Henri, A.-M., Feldman, P. D., et al. 1994, A&A, 290, 245
Williams, J. P., & Andrews, S. M. 2006, ApJ, 653, 1480
Wright, E. L., Eisenhardt, P. R. M., Mainzer, A. K., et al. 2010, AJ, 140, 1868
Wyatt, M. C. 2008, ARA&A, 46, 339
Zuckerman, B., Forveille, T., & Kastner, J. H. 1995, Natur, 373, 494
Zuckerman, B., & Song, I. 2012, ApJ, 758, 77